Environmental Earth Sciences (2022) 81: 436
https://doi.org/10.1007/s12665-022-10556-w

ORIGINAL ARTICLE

Topographic classification of North Eastern Region of India using geospatial technique and following seismic code provisions

Navdeep Agrawal[1] · **Jagabandhu Dixit**[1]

Received: 23 March 2022 / Accepted: 13 August 2022 / Published online: 2 September 2022

Abstract

The availability of high-resolution digital elevation models (DEM) and advancements in geospatial techniques enable a more accurate measure of slope position classes and classification of landforms using algorithms like topographic position index (TPI). In this study, TPI-based slope position classes are used for the identification of major relief features like ridges, and these are embedded with DEM-derived terrain slope to perform the topographic amplification-based classification of the North Eastern Region (NER) of India, according to the present European (Eurocode-8) and Italian seismic codes using GIS tools. They are classified into four topographic classes: T1, T2, T3, and T4. The relation of geological units, seismic site classification map, and land use land cover (LULC) classes with identified topographic classes for the study region are analyzed. The results reveal that ~ 25% of the study area is a potentially high amplification zone (T4 class; amplification factor of 1.4 as per Eurocode-8), primarily associated with dense and light vegetation type land cover. The Indian seismic recording station sites and the epicenters of past earthquake events in the region are classified based on the obtained topographic classification map. Approximately, 47% of earthquake events of large magnitudes and ~ 30% of strong motion network (SMN) station sites are in localities with potential topographic effects. The human settlements are predominantly found in places identified with no or minimal amplification zone (T1 class; amplification factor of 1). The presented topographic classification map of NER can assist the decision-makers and authorities to identify potentially high amplification areas considering seismic hazards and making choices for future infrastructural development.

Keywords Topographic amplification · Seismic site effects · Strong motion station · Topographic position index · DEM · Site classification

Introduction

The influence of site condition on the ground shaking intensity during an earthquake and resulting damage is well known. The rapid infrastructure development and rapid expansion of cities are not limited to the flat grounds and may take place in topographically uneven places like a ridge, mountainous places, etc. (Shabani and Ghanbari 2020). The effect of such topographic features of the site can result in seismic wave amplification or de-amplification (Kramer 1996). The phenomenon of topographic amplification is observed and is well documented during past earthquake events, e.g., 1994 Northridge earthquake of moment magnitude (M_w) 6.7 (USA), 1971 San Fernando earthquake of M_w 6.6 (USA) (Sepúlveda et al., 2005), 2010 Haiti earthquake of M_w 7.0 (Hough et al. 2010), 2016 Norcia earthquake of M_w 6.5 (Italy) (Pignalosa et al. 2022). The topographic features such as hilltops, ridges (or sites close to ridges), or steep reliefs are more susceptible to amplification, whereas de-amplification can occur in the valley/canyon (Lee et al. 2009; Molina et al. 2019; Khan et al. 2020). The seismic amplification due to topographic irregularity is often considered a possible source of earthquake-induced rock sliding, slope failures, or landslides, which can cause widespread damage (Paolucci 2002). Several numerical modeling and experimental studies have investigated surface topographic effects on seismic ground motions (Kawase and Aki 1990; Faccioli et al. 2002; Bouckovalas and Papadimitriou 2005; Del

✉ Jagabandhu Dixit
jagabandhu.dixit@snu.edu.in; jdixitb@gmail.com

Navdeep Agrawal
na655@snu.edu.in

[1] Disaster Management Laboratory, Shiv Nadar University, Gautam Buddha Nagar, Delhi NCR 201314, Uttar Pradesh, India

Gaudio and Wasowski 2011; Gao et al. 2012; Rizzitano et al. 2014; Jafarzadeh et al. 2015; Restrepo et al. 2016; Poursartip et al. 2017; Falcone et al. 2018; Khan et al. 2020; Elyasi et al. 2021; Kumar et al. 2021). The effect of the rate of crustal deformation, geology, local soil deposits, site types, and seismic wave propagation plays a significant role in seismic site effects (Raghukanth et al. 2011; Dixit et al. 2012, 2016; Pan and Jiang 2020; Gupta et al. 2022). However, it is often difficult to quantify the effect of topographic amplification on earthquake damage and its separation from amplification due to the stratigraphic effects (Molina et al. 2019; Falcone et al. 2020a) and near-surface geology (Pessina and Fiorini 2014). A very few seismic design codes of practice for buildings, namely French (Association Française du Génie Parasismique 1990), European (Eurocode-8, EN (2004)), and Italian (NTC, 2018) codes, have only addressed the phenomenon of topographic amplification by introducing an amplification factor based on surface topography (Di Capua et al. 2011; Falcone et al. 2020b). The Indian standard criteria for earthquake-resistant design of structures—general provisions and buildings (IS 1893: Part-1 2016) have not yet included this phenomenon.

The EN (2004) suggests frequency-independent amplification factors based on topographic attributes like relief and slope. It prescribes the amplification factor of not higher than 40% for irregularities of height greater than 30 m with different slope configurations. The Italian code (NTC 2018) also adopted a similar approach, and explicit topographic classes were defined as listed in Table 1 in addition to EN (2004). Following the NTC 2018, a few studies (Di Capua et al. 2011; Pessina and Fiorini 2014; Mascandola et al. 2021) have performed the topographic classification of seismic station sites in Italy (Mascandola et al. 2021) based on high-resolution digital elevation model (DEM). Di Capua et al. (2011) identified the local ridges in the Italian landscape, based on DEM of 30 m × 30 m resolution, using a set of geographic information system (GIS) tools, and a buffer zone of 100 m radius was created around the station sites on which the classification scheme was implemented. Pessina and Fiorini (2014) also adopted a similar procedure with a finer resolution DEM (20 m × 20 m). However, this scheme was unable to classify seismic station sites univocally because the combination of indices (such as slope and ridgeline) in some areas and partially overlaid buffer areas might lead to different classes. Mascandola et al. (2021) suggested a topographic position index (TPI) based ridge detection and proposed a GIS-based procedure for topographic classification of Italian territory, which overcomes the aforementioned limitations. TPI is a very powerful parameter that shows the relative altitude of a site for a defined neighborhood surrounding (Wilson and Gallant 2000) and has been successfully utilized for landform classification combined with topographic attributes, e.g., *slope*, to identify different landform features, ridges, hilltops, and valleys (Weiss 2001; Tağıl and Jenness, 2008; De Reu et al. 2013; Mokarram et al. 2015; Vinod 2017; Nair et al. 2018; Roy and Das 2021).

The complex topographical features and the high seismicity of the Himalayan region, especially the North Eastern Region of India, make it highly vulnerable to human settlements. Many towns and rural settlements are expanding over irregular topographical zones. Therefore, identifying places that may get affected by topographic amplification is an urgent need. In the present study, we performed the GIS-based topographic classification of the North Eastern Region (NER) of India, based on EN (2004) and NTC 2018, following the methodology proposed by Mascandola et al. (2021). For the first time, the same is correlated with sites of strong motion network (SMN) stations in NER (National Center for Seismology, India; Nath et al. 2013), and earthquake events in the region. Along with topographic amplification effects, the stratigraphic effects can influence the seismic hazard parameters (e.g., peak ground acceleration) in the region. Therefore, the zones of topographic amplification obtained are also correlated with the National Earthquake Hazard Reduction Program (NEHRP) site classes for the study area. TPI-based landform classification of NER of India was conducted and the distribution of land use land cover (LULC) classes in the region were analyzed. A detailed discussion about the study area, dataset, steps involved in topographic classification and NEHRP site classification, and results are presented in the subsequent sections.

Table 1 Criteria for slopes and relief features and their topographic amplification factors prescribed by *EN1998-5* (2004) and *NTC* (2018)

As per EN (2004) and NTC (2018)		
Topographic class	Description	Amplification factor
T1	Flat surface, isolated slopes, and cliffs with an average slope angle $i \leq 15°$	1.00
T2	Slopes with average slope angle $i > 15°$	1.20
T3	Relief with ridge width much smaller than the base and average slope angle $15° < i \leq 30°$	1.20
T4	Relief with ridge width much smaller than the base and average slope angle $i > 30°$	1.40

Materials and methods

Study area

The study region consists of the NER of India (except Sikkim), popularly known as the 'Seven-Sister States' of India, covering approximately 253,353 km^2 and includes Arunachal Pradesh, Assam, Manipur, Meghalaya, Mizoram, Nagaland, and Tripura (Fig. 1a). The spatial extent of the region lies between 21° 56′ 46″ N–29° 27′ 48″ N latitudes and 89° 41′ 41″ E–97° 24′ 54″ E longitudes. There exist three tectonic plates in and around NER: the Indian Plate, the Eurasian Plate, and the Burmese Plate (Hurukawa et al. 2012). A relative motion of about 5 cm/year towards the northeast exists between the Indian and Eurasian Plates, leading to the convergence of the Indian plate under the Eurasian plates and active subduction of the Indian plate under the Burmese Plates (DeMets et al. 1994). The physiographic setup of NER of India includes the Himalayan Ranges in the north (over the Indian–Eurasian convergence zone), the Shillong–Mikir plateau in the southwest, and the Indo-Burmese arc along the eastern border, Brahmaputra flood plains in the central and Tripura fold in the south. The Indo-Burmese arc resulted from the interaction between Indian–Burmese plates and is trending NNE–SSE to the south along the international border between India and Myanmar.

The geological setup of the region derived from the United States Geological Survey (USGS) is also shown in Fig. 1b. The geological age of the rocks in NER ranges from Precambrian (Pr) to recent Quaternary sediments. The upper Himalayan portion of the study region (mostly Arunachal Pradesh) generally comprises rocks of the Paleozoic and Mesozoic eras. The Eastern Syntax zone, formed near the junction of Himalayan and Indo-Burmese mountain ranges, includes undivided Precambrian rocks (Fig. 1b). The Brahmaputra flood plains in the Assam valley, trending NNE–SSW, are bounded by the Himalayas in the north, Eastern Syntax in the NE, Shillong–Mikir plateau in the South, and Naga Hills of the Indo-Burmese arc in the SE. It is filled with sediments of the recent era, i.e., Quaternary sediments (Fig. 1b), having a thickness of 3–5 km (Nandy 2001). Overall, Precambrian, Paleogene, Neogene, and Quaternary are the major formations found in NER, as shown in Fig. 1b. The Cenozoic era sedimentary rocks (Tertiary Paleogene and Neogene period) are mainly found in the Southern and SE portions of the study region. Precambrian rocks with some Tertiary sediments of the Paleogene Period in the southeast and Quaternary sediments along the western

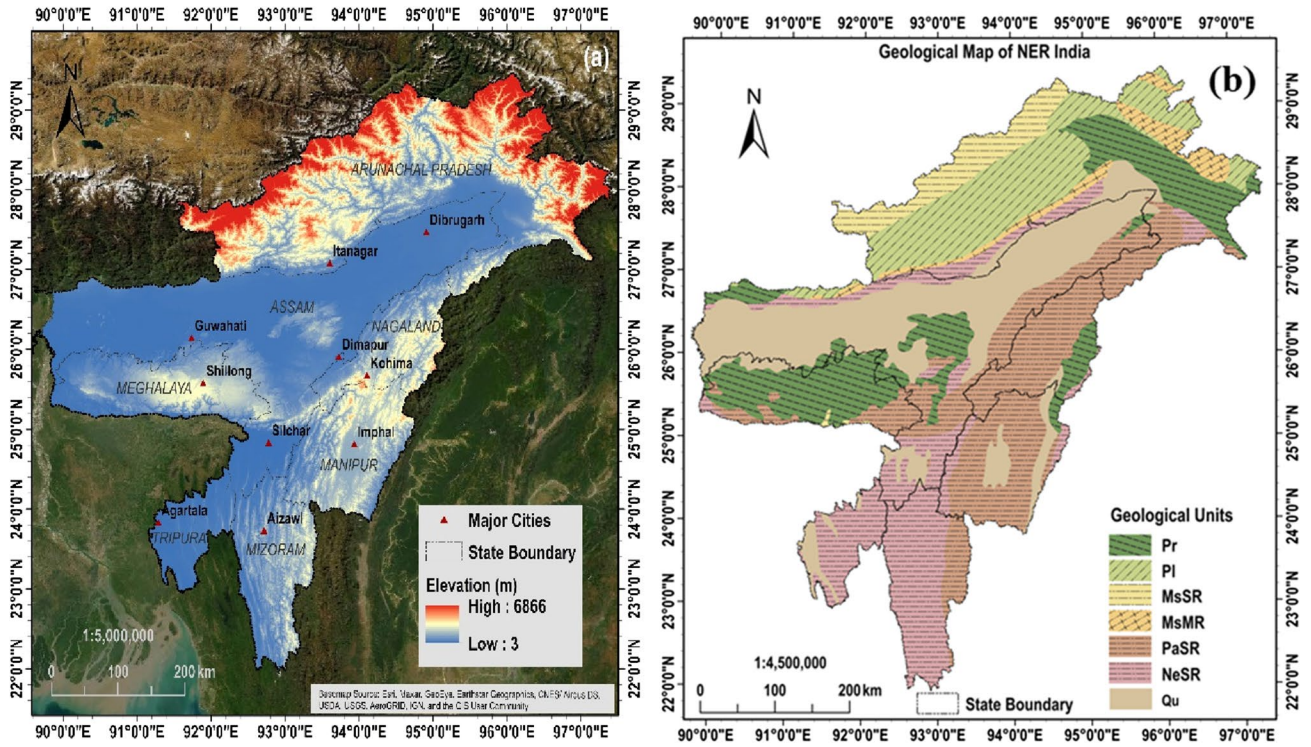

Fig. 1 **a** Study Area: The North Eastern Region of India with ASTER-GDEM v3 derived elevation profile and shaded relief, seven-sister state boundary, and important cities of the region; **b** The geological map of the study area derived from USGS where *Pr* Precambrian; *Pl* Paleozoic; *MsSR* Mesozoic Sedimentary Rocks; *MsMR* Mesozoic Metamorphic Rocks; *PaSR* Paleogene Sedimentary Rocks; *NeSR* Neogene Sedimentary Rocks; *Qu* Quaternary Sediment

portion are primarily found in the Shillong plateau (Kayal and De 1991).

Due to these complex plate tectonics, geological, and resulting physiographic settings, the region is tectonically active and exhibits high seismicity (Sandhu et al. 2020; Agrawal et al. 2022). The entire study area falls under seismic zone V, the most severe zone as per IS (2016), making it suitable for topographic amplification and allied studies. The study can provide insight into risk considering socio-economic indicators (Agrawal et al. 2021).

Dataset and its preprocessing

The present study is based on the 30 m spatial resolution Advanced Spaceborne Thermal Emission and Reflection Radiometer-Global Digital Elevation Model (ASTER-GDEM *v*3), which forms the fundamental basis for morphological analyses (Di Capua et al. 2011). The accuracies and statistical values of the elevation model are shown in Table 2. Before applying to morphological analyses, the DEM was processed (mosaic), and voids were filled using Esri ArcGIS 10.8.1 software (Das et al. 2016; Pham et al. 2018). The dataset was geo-rectified into Universal Transverse Mercator (UTM) projection (zone: 46 N) with World Geodetic System (WGS) 1984 datum. Finally, the DEM was further smoothened to remove any minor irregularities by applying the Focal statistical mean algorithm (in ArcGIS 10.8.1) with a 3 × 3 moving window (Burrough et al. 2015). The slope angle was computed using the *Spatial Analyst Tool* in ArcGIS 10.8.1 on the processed DEM with a projected coordinate system. The statistics of the obtained slope (degrees) for the study area are mentioned in Table 2. The slope map was further classified into three classes, as shown in Fig. 2.

The list of SMN stations and past earthquake events in the region was compiled in the present study. The data regarding seismic stations were obtained from National Center for Seismology (NCS-MOES 2021), India, and from the literature (such as Mittal et al. 2012; Nath et al. 2013; Gupta et al. 2021). A total of 68 SMN station sites were identified with the majority of them located in Assam (37 stations) and Meghalaya (16 stations). Whereas the earthquake catalog was compiled from different sources like NCS-MOES (2021), United States Geological Survey (USGS 2021), and International Seismological Centre (ISC 2021), and only mutually exclusive events are used in the study (Gupta et al. 2021). For the study region, the prepared catalog consists of 2,656 events with the moment magnitude (M_w) ranging from 1.50 to 8.60 in which 1002 events are of M_w 4.0 or above.

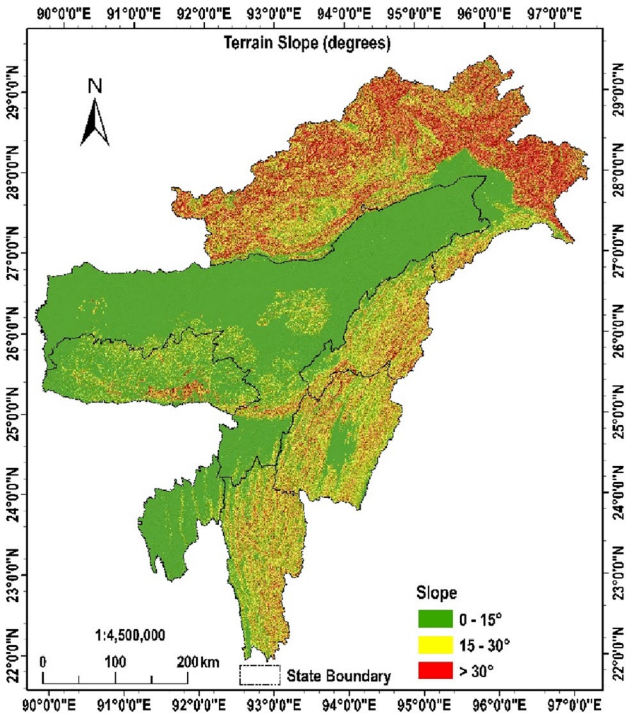

Fig. 2 Terrain slope (in degrees) of NER of India

Table 2 Specification and statistical values for elevation model

DEM specification and statistical values for elevation models		
Data		ASTER-GDEM
Resolution		1 arcsec (~ 30 m)
Vertical accuracy		16.70 m (95%)[a]
Horizontal accuracy		30 m (95%)[a]
Statistical value	Elevation (m)	Slope (degrees)
Minimum	3.00	0.00
Maximum	6866.00	85.50
Mean	960.16	15.70
Standard deviation	1095.06	13.38
Median	570.00	–

[a]AfterGesch et al. (2016)

For the LULC distribution of the study region, the LULC map with *10* classes provided by Esri, which is based on Sentinel-2 (10 m resolution) imagery, was used (Karra et al. 2021). The map was reclassified into *7* classes: (a) agricultural land; (b) bare land/alluvial deposits; (c) dense vegetation/forest cover; (d) human settlement; (e) light vegetation; (f) waterbody; and (g) snow/cloud cover (Gupta and Dixit 2022) and validated by calculating the kappa coefficient (Varade et al. 2019). The ground truth/ validation sample points (a total of 390 points) were obtained (randomly) using Google Earth Pro (for the year 2020) and used to validate the classification (Gupta and Dixit 2022). The developed confusion matrix is shown in Table 3. For the reclassified map, the overall accuracy obtained is 84.1% and the kappa coefficient is 0.814 (Table 3), which indicates that the reclassified and reference images are in good agreement and can be further used in the study (Monserud and Leemans 1992).

Slope position classes and topographic classification

Topographic position index (TPI)

The *TPI*, as proposed by Weiss (2001), compares the elevation of each cell of the DEM layer to the mean elevation of the surrounding cells of a specified scale, as defined in Eq. 1

$$\mathrm{TPI}(r) = \mathrm{Elv}_0 - \frac{1}{n_r}\sum_{i\in r}\mathrm{Elv}_i, \quad (1)$$

where TPI (r) is the *topographic position index* corresponding to a particular neighborhood radius, r (number of cells around the point of interest), Elv_0 is the elevation of the point of interest, i.e., the elevation of the central cell of a circle of radius r, Elv_i is the elevation of the ith cell of the circle of radius r and n_r is the number of cells within that circle.

The large positive *TPI* values ($TPI > 0$) represent the cell that is at a higher elevation than its surroundings (e.g., hilltops and ridges), whereas approximately equal to zero or near zero ($TPI \sim 0$), and negative *TPI* ($TPI < 0$) values, respectively, indicate flat plains or terrain with constant gradients and lower elevation zones than their surroundings (e.g., valleys or basin bottoms). *TPI* is a scale-sensitive parameter; therefore, scale (neighborhood size) and shape (neighborhood type) should be selected in advance, depending upon the application and the feature size (Grohmann and Riccomini 2009). In the present study, the circular neighborhood was adopted. To choose an appropriate neighborhood size, *TPI* values were calculated for *8* different scales, ranging from 5 to 50 units of cells (Pham et al. 2018). For example, the *TPI*05 corresponds to the *TPI* values using the neighborhood scale of a *5*-unit radius (150 m for DEM with 30 m resolution). The results for TPI are shown in Sect. 3.1.

Following Weiss (2001), using the *TPI* and standard deviation of elevation thresholds, the landscape over the study region was classified into 6 distinct slope position classes (SPC). At a smaller scale (e.g., *TPI*05/07/10), the individual ridgelines, hills in the valley, and plains in the valley bottom can be demarcated, whereas, at a larger scale

Table 3 Accuracy assessment of reclassified LULC classes for NER of India

LULC classes	WB	DV	LV	AL	HS	BL	SN	Total (user)	User accuracy (%)[a]	Producer accuracy (%)[a]
WB	61	0	0	0	1	4	1	67	91.04	93.85
DV	0	55	7	1	0	2	0	65	84.62	94.83
LV	0	1	36	8	0	5	1	51	70.59	66.67
AL	1	1	5	53	2	2	0	64	82.81	79.10
HS	0	0	4	3	46	1	0	54	85.19	93.88
BL	3	1	2	2	0	39	0	47	82.98	68.42
SN	0	0	0	0	0	4	38	42	90.48	95.00
Total (producer)	65	58	54	67	49	57	40	390		
Overall accuracy (%)[a]								**84.10**		
Kappa coefficient (k)[a]								**0.81**		

The overall accuracy and kappa coefficient values are made bold

WB Waterbody; *DV* Dense vegetation/forest; *LV* Light vegetation; *AL* Agricultural land; *HS* Human settlement; *BL* Bare land/alluvial deposits; *SN* Snow/Cloud

[a]User accuracy $=(n_{ii}/n_{i+})$; Producer accuracy $=(n_{jj}/n_{+j})$; Overall accuracy $=(1/n)\sum_{i=1}^{c} n_{ii}$; $\mathrm{k}=(n\cdot\sum n_{ii}-\sum(n_{i+}\cdot n_{+j}))/(n^2-\sum(n_{i+}\cdot n_{+j}))$, where n is the total number of samples, c is the number of rows or columns, n_{i+} and n_{+j} denotes the number of sample points in the ith row, and jth column, respectively, n_{ii} is the number of sample point correctly classified in the ith category

(e.g., *TPI*25/30/50), major ridgelines, mountains, and broad valleys can be delineated. For the considered study region, a neighborhood scale of a 15-unit radius (450 m) was adopted, as it allows better delineation of the ridges while ignoring the minor variations in relief features. Further, the TPI-based SPC map was utilized for ridge extraction. For more detailed topography information, nested landform classes can be identified by combining small and large neighborhood scales (Weiss 2001).

The present study obtained the *TPI* and SPC at different scales (05, 07, 10, 15, 20, 25, 30, and 50) using the *Land Facet Analysis* toolbox in ArcGIS 10.8.1 (Jenness et al. 2013). The nested landform classification is performed using *Topography Tools 10.3* in ArcGIS 10.8.1.

Ridge and threshold relief extraction

For ridge delineation in the SPC map, a *TPI* threshold of greater than 5 is selected empirically (Mascandola et al. 2021). As *TPI* reflects the relative elevation, a *TPI* value of 5 means that the cell is 5 m higher than the average elevation of the specified neighborhood. The lower *TPI* thresholds (less than 5 down to 1) are not found to be effective in the areas with less gradient (< 15°). The ridge zones were extracted from the SPC15 (i.e., SPC considering neighborhood size of 15 units) map using the *raster calculator,* and the binary output raster with *1* as ridge zones and *0* otherwise is obtained (Fig. 3a). From this output raster, the ridgelines were extracted by thinning (using the *Thin tool)* the rasterized linear features (ridge zones) as shown in Fig. 3a.

As specified in EN (2004), the features with relief greater than 30 m have a higher potential for site effects due to topographic amplification. Using the Focal Statistics tool, the elevation range in a moving window of size 7 × 7 cells was calculated to identify the cells having relief larger than a specific threshold. To discriminate between topographic classes like T3 and T4, the relief map with a threshold of 30 m and 60 m was extracted. As for a *7* × *7* moving window with DEM of resolution 30 m, for a threshold height of 30 m, the slope angle interval varied from 13.29° to 45° for maximum and minimum distance along the semi-transverse axis (i.e., 90 m$\sqrt{2}$ and 30 m, respectively). Thus, it included both T3 and T4 classes (Table 1). Further, to separate the T4 from T3, the threshold relief of 60 m was considered to have a slope angle ranging from 25.28° to 63°, thus including the ridge sites with relief of more than 30 m and an average slope angle > *30*° as specified in EN (2004).

Identification of threshold relief ridges having potential topographic amplification

After the threshold relief maps (i.e., relief > 30 m; elevation 30) were delineated, the ridgelines corresponding to threshold relief were extracted by overlaying the ridgeline map on relief > 30 m maps (Fig. 3b, c). The extracted ridgelines were processed to remove minor deflections. For this purpose, the *Region Group tool* was utilized, which identifies the scanty group of points having a value other than 0 within the 8-cell neighborhood. The identified groups with less than 5-cell counts were set to null (*Set Null*) and *nibbled* from the ridgeline raster. The output ridgelines were then dilated to 5 cells (150 m) on each side (Fig. 3d), thus incorporating the minimum slope angle threshold of 15° for topographic amplification as per EN (2004).

The final topographic classification map of the study area is prepared by the combination of the slope map, ridge map, and relief map, as shown in a summarized flow diagram (Fig. 4).

Site classification using topographic gradient

Along with topographic classification, the topographic gradient-based site classification (NEHRP site classes) was performed. The procedure suggested by Wald and Allen (2007) was followed to obtain the site classification map. The relationship between topographic gradient and shear wave velocity (V_{S30}) developed by Allen and Wald (2009) was utilized to prepare the site classification map (Table 4). For this purpose, the *1* arc-second DEM data were first resampled to *9* arc-second and employed to obtain the topographic gradient of the study area. The relationships between topographic classes and site classes were analyzed following the site classification.

Further, the locations of SMN stations and past mutually exclusive seismic events in the study region were classified according to the topographic and site classification maps.

Results

The primary outcome of this study is in the form of a topographic classification of the NER of India along with site classification, SPC, and nested landform classification maps. The statistical analysis between the spatial distribution of different SPC and geological units of the study area, between topographic classification map and NEHRP site classes, was performed.

TPI-based slope position classes and nested landform classification

The *TPI* values for 8 different scales were obtained and their spatial distribution is shown in Fig. 5. At a small scale, the spatial variation of *TPI* is not obvious, while at a larger scale, the major hills and ridgelines are apparent. Also, the value range increases sharply with the scale from 5 to 15,

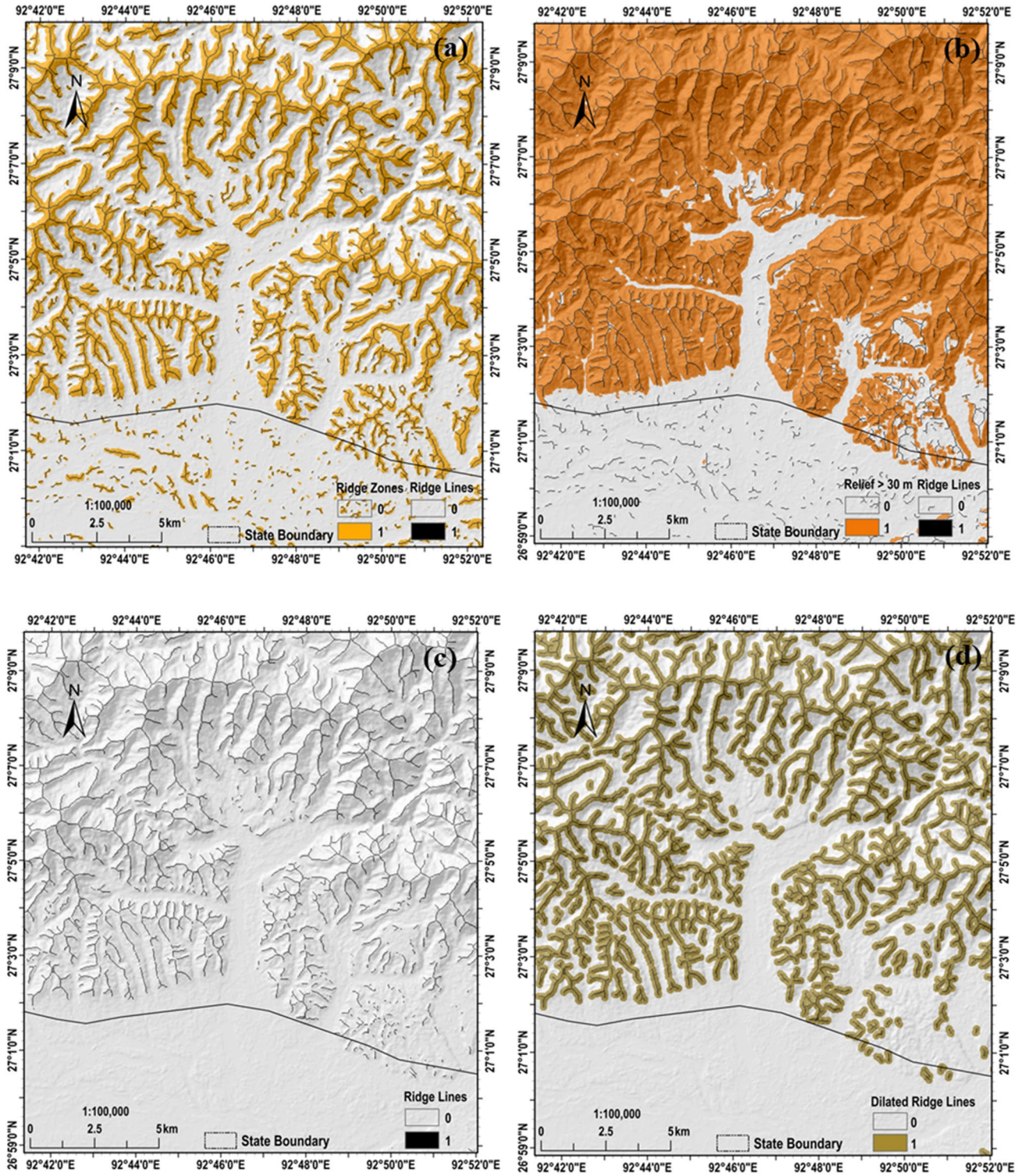

Fig. 3 **a** Ridge zones and ridgelines after thinning; **b** Ridgeline map overlaying on Relief > 30 m map; **c** Extracted ridge lines intersected with Relief > 30 m; **d** Dilated ridgelines, presenting Ridge map with shaded relief

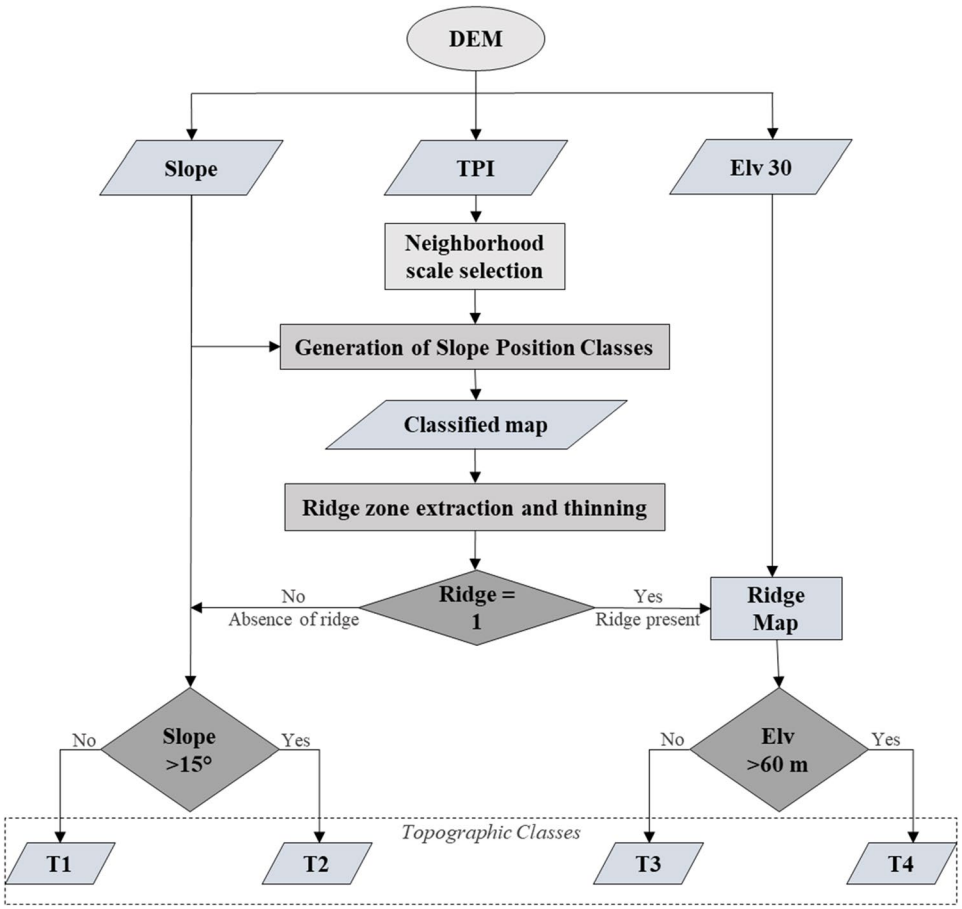

Fig. 4 Flow diagram for topographic classification

Table 4 Correlation between topographic gradient and shear wave velocity (V_{S30}) for *NEHRP* site classes (after Allen and Wald 2009)

9 arcsec topographic gradient range (m/m)	V_{S30} range (m/s)	NEHRP site class
$<3\times10^{-4}$	<180	E
3×10^{-4}–3.5×10^{-3}	180–240	D
3.5×10^{-3}–0.010	240–300	
0.010–0.024	300–360	
0.024–0.08	360–490	C
0.08–0.14	490–620	
0.14–0.20	620–760	
>0.20	>760	B

attaining the maximum in the case of *TPI* 15, and then starts decreasing gradually with further increase in scale, forming a bell-shaped curve (Fig. 6).

The influence of neighborhood cell size (*TPI* scale) is observed on the SPCs (Fig. 7 and 8). At a smaller neighborhood radius, features like flat area/gentle slope, steep slope, and upper slopes are better presented (Fig. 8). The category like valley and ridges are found to be the largest category, covering together approximately 42% (at *5-cell* neighborhood) to 74% (at *50-cell* neighborhood) of the study area. The percentage distribution of each SPC with respect to the scale is illustrated in Fig. 7. Visual observation reveals that all the landscape features (SPCs) are well represented in the case of neighborhood radii of *15 units* which are also justified by the maximum observed *TPI* range using this radius. At this scale, approximately 65% of the area is identified as valleys and ridges, and the other four categories occupy the remaining 35%. Overall, the smallest portion of the area falls under the steep slope category in all the cases. The proportion is almost negligible at neighborhood radii of *30* and *50 units*. Also, with an increase in scale up to *15 cell units*, the sharp decrease in the proportion of area categorized as flat plain/gentle slope and the upper slope is observed, while at larger scales like *25* and more, the reduction is minimal. Most of the flat plain area is concentrated along the Brahmaputra flood plains (Assam region) portion of the study region (Fig. 8).

As smaller features are better presented at smaller radii, while the larger feature is dominating at a larger scale. The entire study region is classified into 10 nested landform classes (in Fig. 9), by combining the small (TPI 05) and large (TPI 25) neighborhoods (Roy and Das 2021). The percentage distribution of each class is shown in Fig. 10.

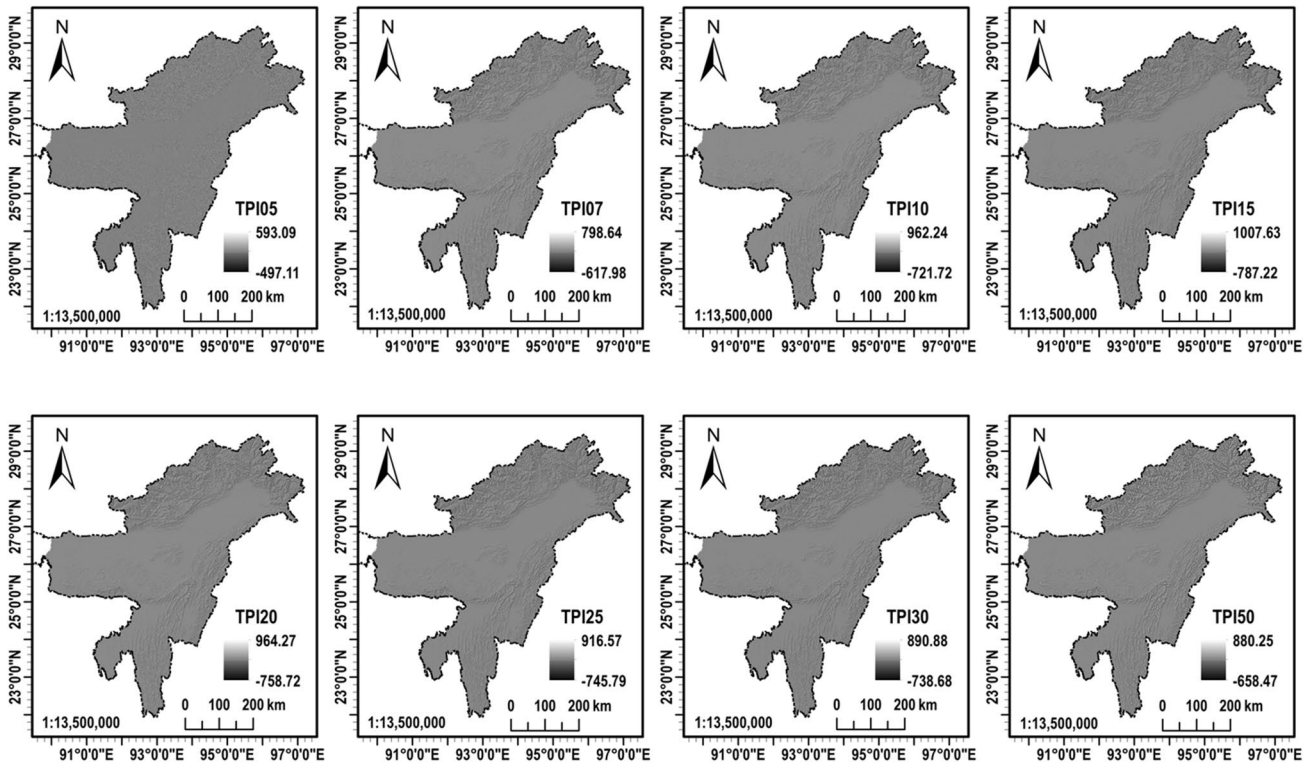

Fig. 5 Topographic position index (*TPI*) for the NER of India based on different scales (number of neighborhood cells)

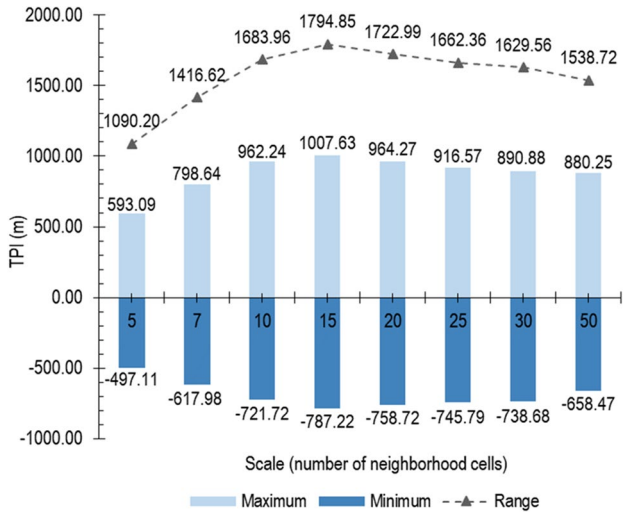

Fig. 6 Variation of *TPI* output for different selected scales

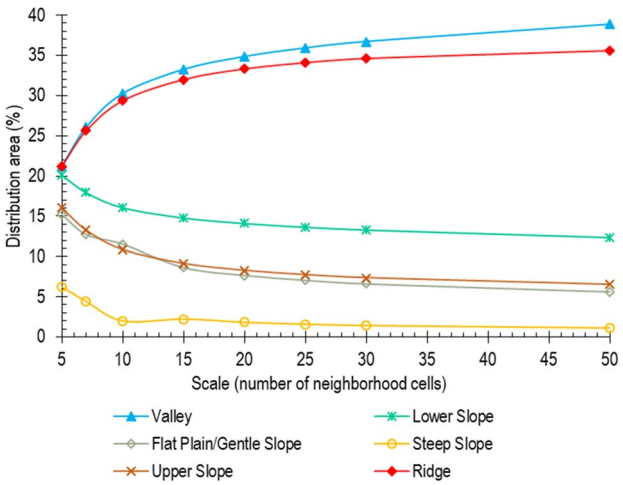

Fig. 7 Areal distribution of different SPC based on *TPI* of selected eights scales (5, 7, 10, 15, 20, 25, 30, and 50 units)

The high-altitude regions are dominated by mountain tops, high ridges, and canyons/deeply incised streams occupying more than 45% of the study region (Figs. 9 and 10). While, the categories like plains, open slopes, and wide valleys (U-shaped valleys) are primarily identified in the Assam region (Fig. 9) and have quaternary sediments as a significant geological unit in these landform features (Table 5). In the case of plains, most of it was quaternary sediments (74.60%, Table 5). The features like midslope/shallow valleys, open slope, and midslope ridges together occupy less than a 3.50% portion of the study region (Fig. 10).

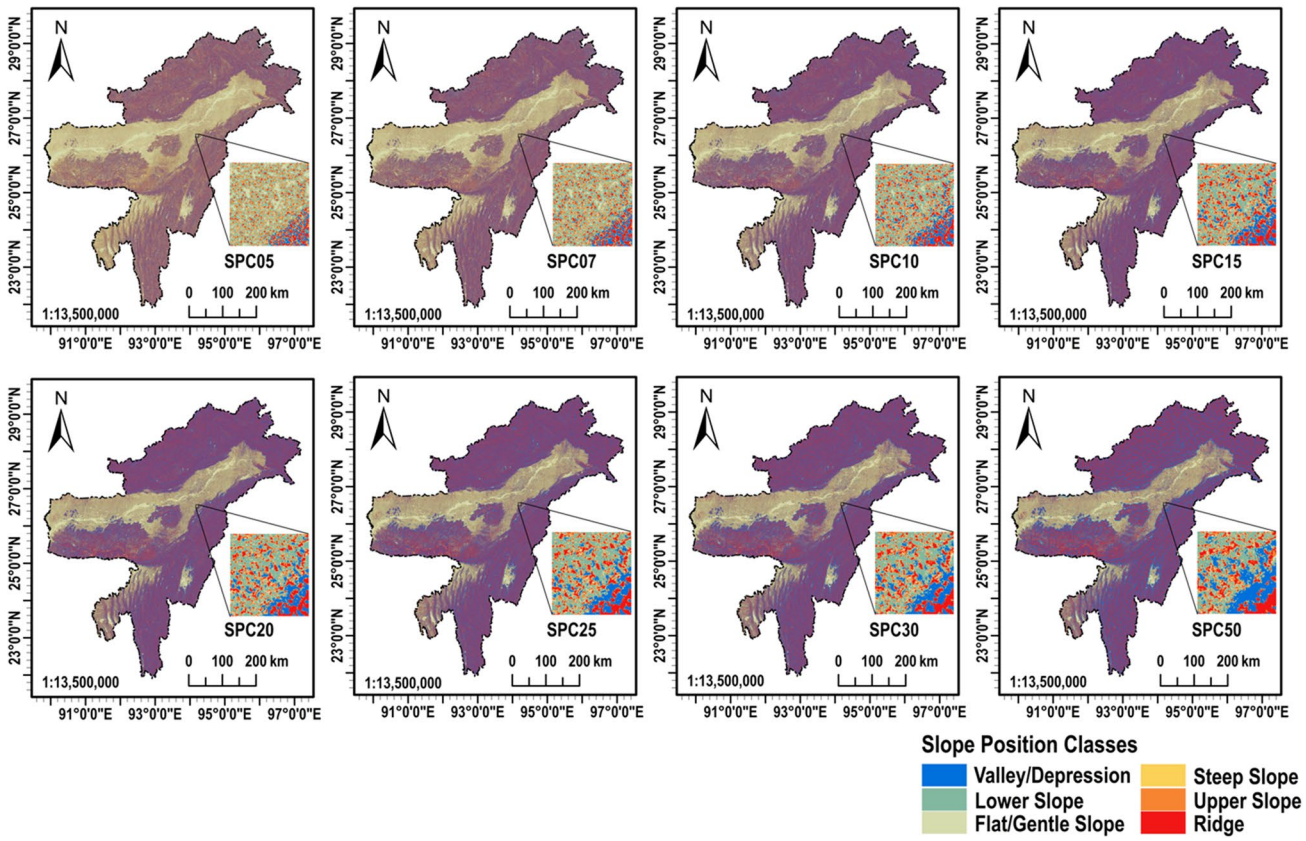

Fig. 8 *TPI*-based slope position classification for selected eight neighborhood scales

Topographic amplification factor-based topographic classification map

The topographic amplification factor-based classification map is represented in Fig. 11. A significant portion of the study area, about 25%, falls under T4 ridges (having an amplification factor of 1.40 as per EN (2004). The largest proportion of the study area is identified as T1 (45.50%), mainly in Assam, Meghalaya, and Tripura. The state-wise distribution of topographic classes reveals that Assam and Tripura are characterized predominantly by T1 slopes (87.80% and 89.66%, respectively) and second-most by T3 ridges (5.00% and 5.60%, respectively). The portion of the Himalayas in the study region, i.e., falling in Arunachal Pradesh, is characterized by prevalent T4 ridges (43.26%) and T2 slopes (38.69%) (Fig. 11).

The states along the Indo-Burmese arc, like Manipur, Mizoram, and Nagaland, are having T4 ridges as the predominant class with around 37% each (Fig. 11) and T2 slopes as the second-most prevalent category (ranges from 30.00 to 31.60%). Overall, approximately 30% area of the considered study region is characterized by T2 or T3 classes (amplification factor of 1.20, Table 1) (Fig. 11).

The distribution of identified topographic classes for the NER of India was analyzed for observed earthquake events over the last 270 years (2656 events). A seismic event was distributed according to topographic classification and the corresponding events were grouped into four (4) moment magnitude (M_w) ranges (i.e. < 4.0, 4.0–5.0, 5.0–6.0, and > 6.0) as represented in Fig. 12. The epicenter of many seismic events irrespective of specific magnitude range was found in the localities of the T1 slope category (~ 43%; 1149 events), followed by T4 ridges (~ 25%; 660 events) (Fig. 13). In the case of locations with a higher magnitude range ($M_w > 6.0$), ~ 52% of such locations were under T1 (11 events), and more than 47% were under the influence of topographic amplification (T2 (~ 28%; 6 events) and T4 (~ 19%; 4 events) topographic classes) (Table 6). However, for events of size more than M_w 5.0, ~ 57% of localities were falling under T2, T3, or T4 topographic classes (affected by topographic amplification, Table 6). The statistics of earthquake magnitudes for different topographic classes are presented in Table 7. For all topographic classes, the median magnitude value ranges from M_w 3.7 to 3.8.

Along with the seismic events, the seismic recording stations present in the study region were also classified according to topographic classes, as in Fig. 14. The database of

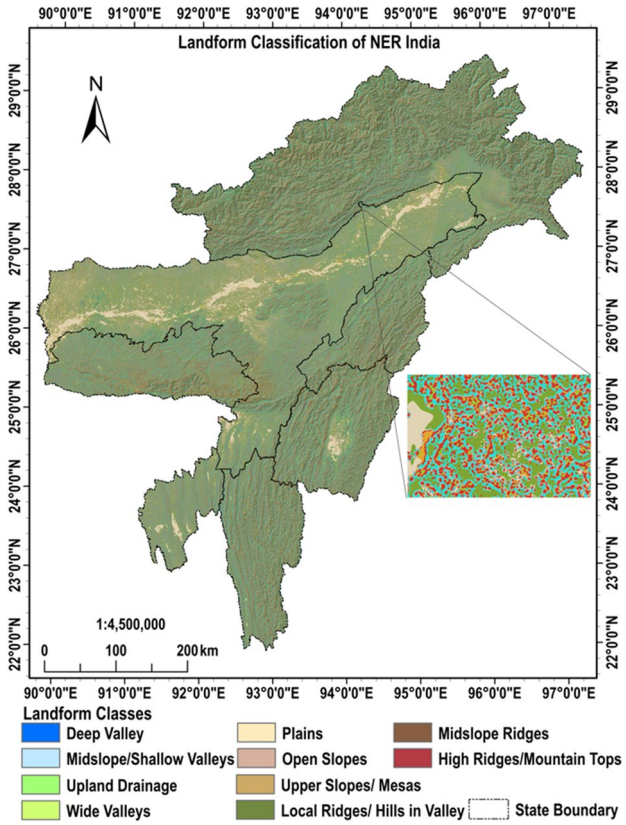

Fig. 9 Landform classification of NER, based on TPI 05 and TPI 25

Indian SMN stations is listed in NCS-MOES (2021) and Nath et al. (2013) and operated by the Department of Earthquake Engineering, IIT Roorkee (Table 8). As many station sites were found in the Assam region only (which have ~ 89% area as T1, Fig. 12, Table 8). Approximately, 70% of SMN station sites were classified as T1 against only ~ 6% of station sites as T4 class (Fig. 14). When the sites of these stations were mapped for geology, 34% were on Precambrian sites, 24% were on Paleogene sedimentary rocks, 19% and 18% were on Neogene sedimentary rocks and Quaternary sediments, respectively, while the remaining 6% were on other geological units (Table 9).

Topographic gradient-based site classification and its comparison with identified topographic classes based on NTC2018

The site classification was performed using a topographic gradient-based approach (Allen and Wald 2009). Figure 15 depicts the proposed site classification map for the NER of India. In the present study, ~ 41% of sites are identified as NEHRP site class B ($V_{S30} > 760$ m/s), followed by site classes C and D (~ 29% each) (Fig. 15). The summary of site class definition is shown in Table 4. When the site classification map is compared with the topographic classification map, more than 99% of the area of site class E ($V_{S30} < 240$ m/s) and ~ 99% of the area of site class D (240 m/s $< V_{S30} > 490$ m/s) are falling under topo-class of T1 (Fig. 16). For site class B, ~ 49% area is of category T4, and ~ 43% area is of T2. Whereas, in the case of site class C, the distribution of topographic classes ranges from 14.68% to 48.22%, as shown in Fig. 16.

The site classification of SMN stations (Table 8) was obtained by comparing it with the site classification map in Fig. 16. The percentage distribution of seismic station sites with respect to topographic class and site class is shown in Fig. 14. 49% of station sites are identified as site class C, of which 58% are of T1 class (Table 10). The stations on site class D are mainly categorized as T1 (Fig. 14). Out of all station sites, ~ 41% of sites are of class D, of which ~ 96% are associated with T1.

For the NER of India, very few studies are available that compare the SMN station sites with the site classification (Mittal et al. 2012; Nath et al. 2013; Sandhu et al. 2020). In

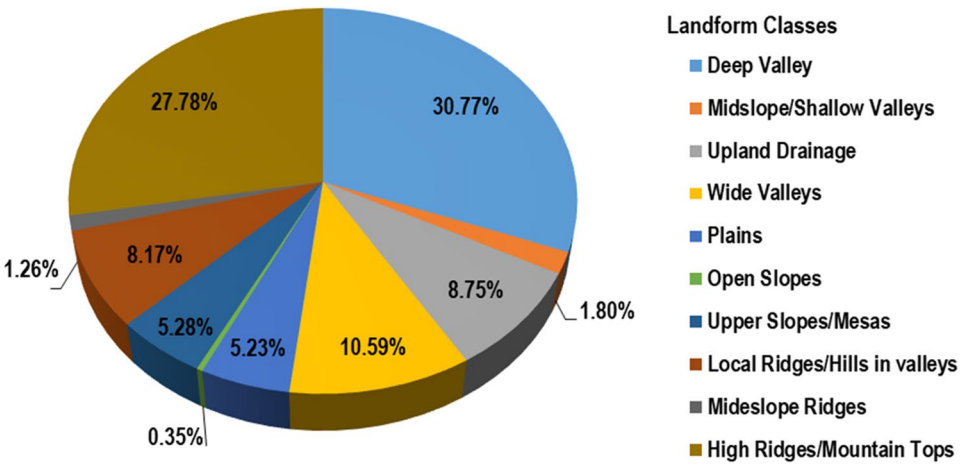

Fig. 10 Areal distribution (%) of different landform classes

Table 5 Areal distribution of geological units according to different landform

Landform classes	Area-wise (%) geological units						
	Pr	Pl	MsSR	MsMR	PaSR	NeSR	Qu
Deep valley	18.23	14.94	5.48	3.66	23.65	18.16	15.88
Midslope/shallow valleys	13.79	4.11	1.27	1.24	18.16	16.49	44.95
Upland drainage	19.72	18.45	7.42	4.39	23.67	16.53	9.82
Wide valleys	12.47	5.27	1.90	1.33	18.37	15.51	45.15
Plains	6.82	0.81	0.02	0.36	7.85	9.55	74.60
Open slopes	15.80	4.25	1.50	1.09	23.03	20.41	33.91
Upper slopes/mesas	16.77	9.09	3.59	2.16	20.18	16.30	31.90
Local ridges/hills in valleys	19.04	19.77	7.10	4.48	25.06	16.98	7.57
Midslope ridges	15.34	5.78	1.68	1.50	20.52	19.28	35.89
High ridges/mountain tops	18.54	15.73	5.80	3.73	23.02	17.37	15.80

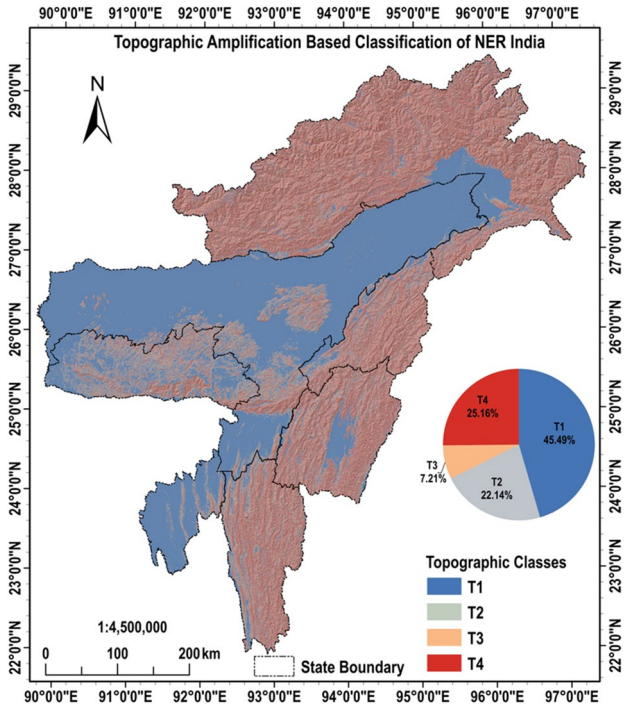

Fig. 11 Topographic classification as per EN (2004), and its percentage distribution for NER of India

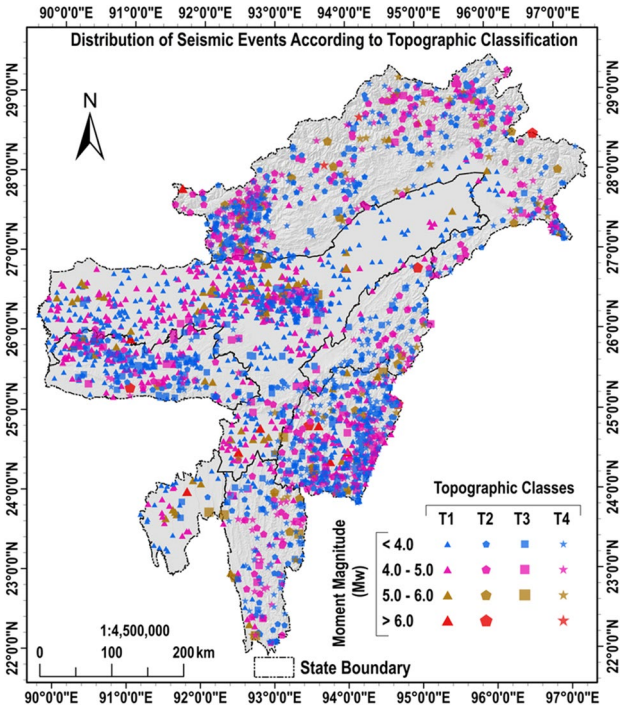

Fig. 12 Distribution of seismic events according to topographic classification

the present study, the identified site classes are compared with the study by Nath et al. (2013). For Arunachal Pradesh, based on NCS-MOES (2021), 6 sites of the stations are identified which were not considered in the other reported studies. Most of the station sites of Arunachal Pradesh are found to be associated with site class C (5 out of 6). Whereas, for Assam, the classification is found to be comparable with the other reported study and a majority of them are falling under site class D in the present study (Table 8). For station sites in Manipur, Mizoram, Nagaland, and Tripura, the site classification of station sites is not reported earlier (Nath et al. 2013; Sandhu et al. 2020). The sites of Manipur, Mizoram, and Nagaland are generally found to be associated with site class C or B (showing rock or hard rock sites). The station sites in Tripura (having relatively younger geological age) are found with site class D (representing deposits of loose to medium cohesionless soil). However, in the case of Meghalaya, inconsistent results are observed. As the Meghalaya is over a plateau region, the variation in slope is less, and therefore, the topographic gradient-based approach perhaps resulted in such observation. Overall, this approach can be utilized for region-specific first-generation NEHRP site classification, especially for remotely inaccessible areas. The

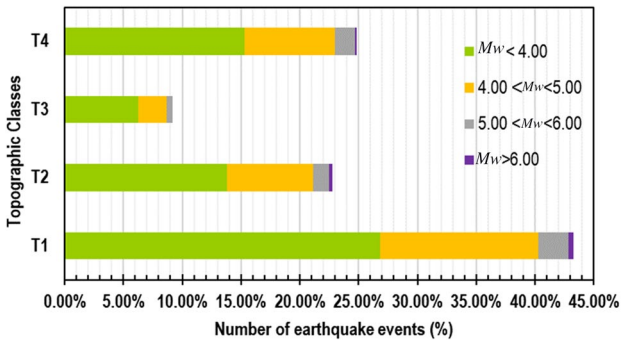

Fig. 13 Distribution of the different magnitudes of earthquakes according to topographic classes

Table 6 Classification of the observed number of earthquake events in NER of India for different topographic classes

Topographic classes	Earthquake events			
	$<M_w$ 4.0	M_w 4.0–5.0	M_w 5.0–6.0	$>M_w$ 6.0
T1	713	356	69	11
T2	367	194	37	6
T3	167	64	12	0
T4	407	203	46	4

Table 7 Statistics of earthquake magnitude (M_w) for different topographic classes

	T1	T2	T3	T4
Min	1.50	2.40	1.70	1.80
Q1	3.30	3.30	3.20	3.30
Median	3.80	3.80	3.70	3.80
Q3	4.30	4.40	4.20	4.40
Max	8.10	8.60	6.00	6.70
Mean	3.90	3.90	3.70	3.90
Range	6.60	6.20	4.30	4.90

approach can be further improved by updating the empirical relation for a finer resolution DEM dataset.

Comparison of topographic classes and site classes with the LULC classes

The LULC classification of the study area and its percentage distribution is shown in Fig. 17. The most dominant feature is forest cover/dense vegetation (69.2%), followed by agricultural land (12.43%), light vegetation cover (7.53%), patches of human settlement (5.53%), bare land/alluvial deposits (2.02%), waterbody (1.75%) and snow/cloud cover (1.54%, concentrated in the upper Himalayas in Arunachal Pradesh). Most

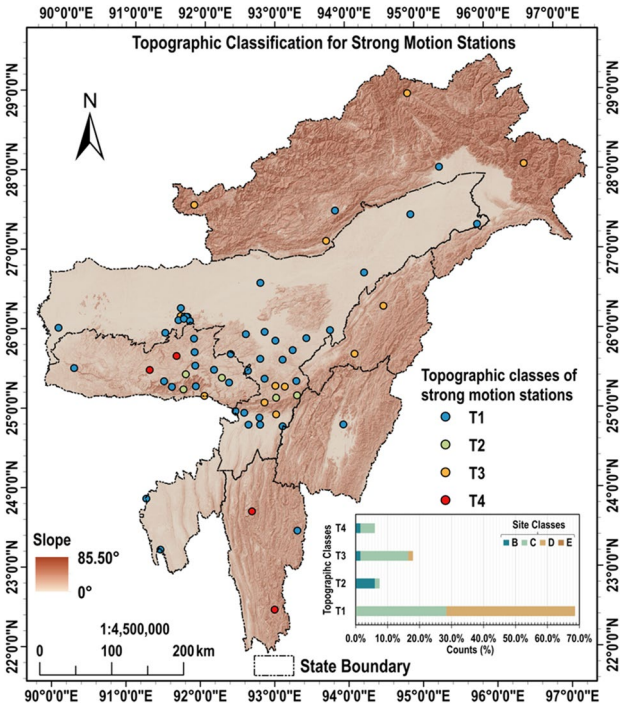

Fig. 14 Topographic classification of Indian SMN station sites in the NER of India

of the human settlement locations and agricultural lands are concentrated in Assam compared to the rest of the study region (Fig. 17). The comparison of the LULC image with the derived topographic classification map for the study area shows that most of the human settlement patches (~94%) and ~99% of agricultural lands are in the category of T1. Whereas, the sites that may be affected by topographic amplification (i.e., T2, T3, or T4 classes) are generally associated with dense vegetation/forest cover or light vegetation (~88% and ~7.5%, respectively, in all three cases) (Table 11). The comparison with site classification shows that most human settlement locations are on site class D (82.8%) or C (14.16%), which may pose a significant risk during a seismic event due to possible ground amplification (Table 12). However, as the human settlement locations are mostly on T1 slopes (Table 11), the effect due to topographic amplification may not be of much concern in these localities.

Discussion

The main scope of this study was to develop the topographic amplification-based topographic classification map of the NER of India according to available seismic code provisions. The influence of topographic amplification on seismic ground motions, i.e., topographic effects,

Table 8 Details of SMN stations with coordinates, geology, SPC, and identified NEHRP site class

S. no.	Station	State	Latitude (°)	Longitude (°)	Geology[a]	SPC[b]	Site Class (present study)	Site Class (Nath et al. 2013)[c]
1	Hayuliang	Arunachal pradesh	28.082	96.525	Pr	1	B	–
2	Itanagar		27.144	93.722	Qu	6	C	–
3	Pasighat		28.061	95.326	Qu	6	C	–
4	Tawang		27.594	91.867	MsSR	6	C	–
5	Tuting		28.994	94.892	Pl	6	C	–
6	Ziro		27.526	93.850	Pl	4	C	–
7	AEC	Assam	26.141	91.661	Pr	1	C	D
8	Amtron		26.185	91.786	Qu	1	C	C
9	Baigaon		25.410	92.860	PaSR	6	C	C
10	Baithalangso		25.970	92.600	Qu	2	D	D
11	Bamun Gaon		25.890	93.010	PaSR	3	D	D
12	Bokajan		26.020	93.770	PaSR	1	D	C
13	Borlangfer		25.770	93.250	NeSR	1	C	C
14	Cotton		26.187	91.743	Pr	5	D	E
15	Dhubri		26.020	89.995	Qu	6	D	–
16	Dibrugarh		27.468	94.911	Qu	3	D	–
17	Dipu		25.920	93.440	NeSR	2	D	C
18	Doloo		24.920	92.790	NeSR	3	D	C
19	Gunjung		25.320	93.010	PaSR	6	C	C
20	Guwahati		26.193	91.691	Pr	6	D	E
21	Haflong		25.170	93.020	PaSR	6	B	C
22	Hajadisa		25.380	93.300	PaSR	1	C	C
23	Harangajao		25.110	92.860	PaSR	6	C	C
24	Hatikhali		25.650	93.110	Pr	5	D	C
25	Hojai		26.000	92.860	Pr	3	D	D
26	IITG		26.293	91.692	Qu	5	D	E
27	IRRIG		26.184	91.772	Qu	2	C	D
28	Jalalpur		25.000	92.460	NeSR	2	C	C
29	Jirighat		24.810	93.110	NeSR	2	D	D
30	Jorhat		26.743	94.251	PaSR	4	D	–
31	Kalain		24.980	92.580	NeSR	1	D	C
32	Katakhal		24.830	92.640	Qu	3	D	C
33	Koomber		24.960	93.020	NeSR	1	C	C
34	Lekhapani		27.333	95.846	PaSR	2	D	–
35	Liasong		25.200	93.310	NeSR	1	B	C
36	Loharghat		25.980	91.480	Pr	2	D	D
37	Maibang		25.310	93.140	PaSR	6	C	C
38	Panimur		25.660	92.800	Pr	6	D	C
39	RRL		26.158	91.736	Pr	2	D	D
40	SD		26.132	91.821	Qu	2	D	D
42	Silchar		24.830	92.800	NeSR	2	D	D
43	Tezpur		26.617	92.800	Qu	6	C	–
44	Umrangso		25.510	92.630	PaSR	2	D	B+
45	Imphal	Manipur	24.831	93.946	PaSR	6	C	–

Table 8 (continued)

S. no.	Station	State	Latitude (°)	Longitude (°)	Geology[a]	SPC[b]	Site Class (present study)	Site Class (Nath et al. 2013)[c]
46	Cherapunji	Meghalaya	25.270	91.740	Pr	6	B	B +
47	Dauki		25.190	92.030	MsSR	6	C	C
48	Jowai		25.420	92.270	Pr	5	C	C
49	Khliehriat		25.360	92.370	PaSR	2	D	B +
50	Mawkyrwat		25.370	91.470	Pr	1	C	B +
51	Mawphlang		25.460	91.770	Pr	6	B	B +
52	Mawsynram		25.300	91.580	Pr	6	C	B +
53	Nongkhlaw		25.690	91.640	Pr	6	C	B +
54	Nongpoh		25.910	91.880	Pr	1	C	B +
55	Nongstoin		25.510	91.270	Pr	6	C	B +
56	Pynursla		25.310	91.910	Pr	1	C	B +
57	Saitsama		25.720	92.390	Pr	1	D	C
58	Shillong		25.570	91.900	Pr	2	C	B +
59	Tura		25.517	90.224	Pr	1	C	–
60	Ummulong		25.520	92.160	Pr	2	D	B +
61	Umsning		25.740	91.890	Pr	1	C	B +
62	Aizawal	Mizoram	23.738	92.690	NeSR	6	C	–
63	Champai		23.495	93.310	PaSR	6	C	–
64	Saiha		22.500	93.000	NeSR	6	B	–
65	Kohima	Nagaland	25.720	94.108	PaSR	6	C	–
66	Mokokchung		26.321	94.516	PaSR	6	C	–
67	Agartala	Tripura	23.889	91.246	Qu	5	D	–
68	Belonia		23.248	91.447	NeSR	2	D	–

[a]Typical geology of the station site based on obtained Geological Map from USGS for the study region (Fig. 1b), where Pr: Precambrian; Pl: Paleozoic; MsSR: Mesozoic Sedimentary Rocks; PaSR: Paleogene Sedimentary Rocks; NeSR: Neogene Sedimentary Rocks; Qu: Quaternary Sediment

[b]Identified Slope position classes based on SPC15, where 1: Valleys; 2: Lower Slopes; 3: Flat/Gentle Slopes; 4: Steep Slopes; 5: Upper Slopes; 6: Ridges

[c]The site class B^+ was used by Nath et al. (2013), for sites with $V_{S30} \geq 760$ m/s

Table 9 Distribution (%) of SMN stations in different geological units according to topographic classes

	SMN station sites (%)							
	Geological units	Pr	Pl	MsSR	MsMR	PaSR	NeSR	Qu
Topographic classes	T1	23.53	1.47	0.00	0.00	14.71	13.24	16.18
	T2	4.41	0.00	0.00	0.00	1.47	1.47	0.00
	T3	2.94	1.47	2.94	0.00	7.35	1.47	1.47
	T4	2.94	0.00	0.00	0.00	0.00	2.94	0.00

has been well observed and reported in the past (Sepúlveda et al. 2005; Molina et al. 2019). Only a few seismic codes have addressed this issue of topographic amplification by introducing the amplification factor as a function and configuration of topographic features such as slope, ridge, and a relief threshold (EN 2004; NTC 2018). Although the provisions are oversimplified and period independent, considering the amplification phenomenon using the topographic amplification factor will allow appropriate seismic load calculation at hilltops, ridges, or crests.

Following the Eurocode-8 (EN 2004) and NTC (2018), the topographic classification of NER of India was performed. For this purpose, a GIS-based methodology proposed by Mascandola et al. (2021) was followed. The topographic features such as ridges in the study area were identified by performing *TPI*-based slope position landform

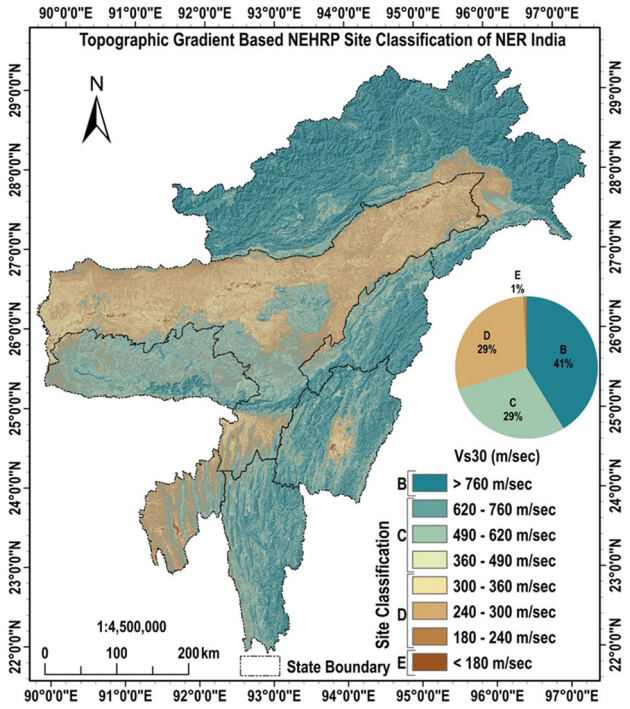

Fig. 15 Topographic gradient-based site classification for the NER of India

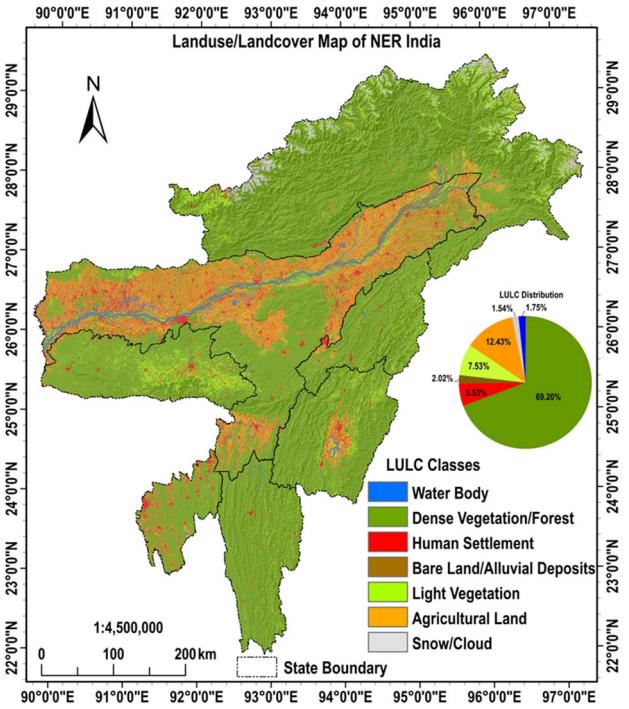

Fig. 17 LULC map of the NER of India along with areal distribution of LULC classes

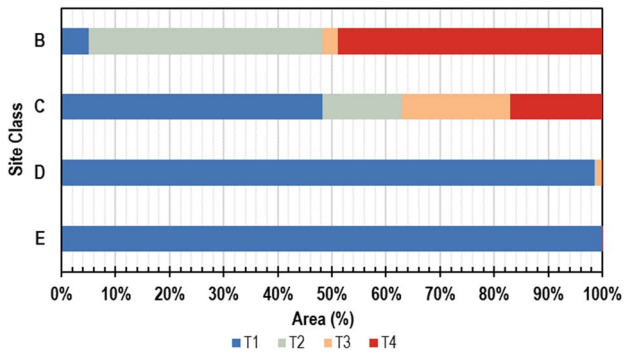

Fig. 16 Areal distribution of topographic classes according to NEHRP site classes for NER of India

Table 10 Number of SMN stations in different NEHRP site classes w.r.t. topographic classes

	Number of SMN stations				
	Site class	B	C	D	E
Topographic classes	T1	0	19	27	0
	T2	4	1	0	0
	T3	1	10	1	0
	T4	1	3	0	0

classification with varying neighborhood cell numbers (scale). A neighborhood size of 15 units radii (450 m) was found to be appropriate for ridge detection based on the visual comparison (Roy and Das 2021). The *TPI* statistics also confirmed this selection (Fig. 6). Based on SPC15, the most dominating topographic features of the study area are ridges and valleys (covering 65% area), concentrated along the Himalayan arc and Indo-Burmese ranges. The nested landform classification also shows similar results. Most sites that may be potentially affected by topographic amplification (i.e., T2, T3, or T4) are generally found in these regions (Fig. 11). The areas, namely Assam and Tripura are having flat/gentle slopes and lower slopes as the dominant SPCs, and therefore, are found with the highest share of T1 slopes, i.e., the topographic amplification effect potentially is minimal as per EN 1998-5 (Di Capua et al. 2011). Overall, ~ 55% area shows potential for topographic site effects.

The identified topographic class are further compared with the NEHRP site classes and LULC classes in the region. In the case of NEHRP site classification using a topographic gradient-based approach, site classes B and C are generally associated with T3 or T4 classes. The DEM data-based site classification is less time-consuming and effective. The topographic gradient has been used as a proxy for site classification and performed satisfactorily in the earlier studies (Nath et al. 2013; Cannon and Dutta 2015). In this study, except for the sites in the Plateau region, the site classification of

Table 11 Relation between LULC and topographic classes

Topographic classes	LULC classes							
	Waterbody	Dense veg	Human settlement	Bare land	Light veg	Agricultural land	Snow/cloud	Total
T1	3.76	46.42	11.38	3.65	7.39	27.19	0.20	100
	97.65	30.52	93.59	82.05	44.66	99.53	6.05	
T2	0.09	88.33	0.28	0.73	7.75	0.04	2.77	100
	1.20	28.27	1.13	7.99	22.78	0.07	39.90	
T3	0.22	87.98	2.61	0.27	7.63	0.61	0.69	100
	0.91	9.16	3.40	0.95	7.30	0.35	3.23	
T4	0.02	88.16	0.41	0.73	7.56	0.02	3.10	100
	0.25	32.05	1.88	9.01	25.26	0.04	50.82	
Total	100	100	100	100	100	100	100	

The values are representing the percentage area. The top value of each cell (shaded rows) represents the distribution of LULC classes according to topographic classification, while the unshaded cells (bottom values) represent the distribution of topographic classes according to LULC classes

Table 12 Relation between LULC and site classes

Site classes	LULC classes							
	Waterbody	Dense veg	Human settlement	Bare land	Light veg	Agricultural land	Snow/cloud	Total
E	20.89	8.52	4.18	28.43	10.63	27.31	0.04	100
	8.77	0.09	0.56	10.36	1.04	1.62	0.02	
D	4.58	29.58	15.70	4.60	5.88	39.64	0.01	100
	76.30	12.48	82.80	66.48	22.83	93.09	0.16	
C	0.74	84.90	2.72	0.51	8.19	2.26	0.67	100
	12.09	35.32	14.16	7.25	31.36	5.25	12.76	
B	0.12	87.40	0.33	0.78	8.16	0.01	3.20	100
	2.85	52.12	2.48	15.91	44.78	0.05	87.06	
Total	100	100	100	100	100	100	100	

The values are representing the percentage area. The top value of each cell (shaded rows) represents the distribution of LULC classes according to NEHRP site classification, while the unshaded cells (bottom values) represent the distribution of NEHRP site classes according to LULC classes

Indian SMN station sites is comparable with other studies. Several studies have performed SMN station site classification based on different classification schemes. Mittal et al. (2012) simply classified the station sites into three classes: A, B, and C, and Nath et al. (2013) adopted a classification scheme with 4 categories based on the NEHRP site classes. Sandhu et al. (2020) proposed modified site classification after Mittal et al. (2012) and classified SMN station sites into 4 classes. Due to this reason, the identified site classes of SMN stations of the NER India in the present study differ slightly and variations in classified sites are observed (Mittal et al. 2012). However, for remote and inaccessible localities, the topographic gradient-based site classification approach can be adopted.

The localities with potential for topographic effects, when compared with its LULC classes, are generally found with either dense or light vegetation cover. The majority of human settlement (or built environment) patches are not found associated with the potential for topographic amplification in the NER of India. However, the proximity of these locations to landscape features like a hilltop, the ridge can significantly impact the hazard potential during an earthquake event and needs to be further investigated (Assimaki and Gazetas 2004). For the sites in the potential topographic amplification zone, i.e., in the T2, T3 or T4 class, a more rigorous evaluation of seismic site performance must be performed considering the seismic site effects. Further, the results of the present study can be used as an extra tool in seismic risk reduction policies, planning critical infrastructure, future

land use development, and densifying the existing SMN station array in the region.

Conclusion

TPI-based landscape analysis and classification is very cost-effective and time-saving, as it provides preliminary information about topographic features and their arrangements in a region, rationally. The *TPI* derived from ASTER-GDEM v3 (30 m resolution) is used to identify the landscape features. Some landform features such as hilltops and ridges can amplify the ground motion during a seismic event other than the site amplification effects. The complex plate tectonics, physiography, and high seismicity of the NER of India make the region highly vulnerable to seismic site effects. In the present study, the topographic amplification-based classification map is developed for one of the most seismic active regions of the world, the NER of India, according to seismic code provisions (EN 2004; NTC 2018). The map shows that approximately 55% area in the study region has potential for topographic effects (associated with T2, T3, or T3 class). Most of these localities are in the upper Himalayas and Indo-Burmese arc, where ridges and valleys are identified as the most dominant landscape features and generally have dense and light vegetation type LULC. The majority of human settlement patches (~94%) of the region are in the plains/gentle slopes with T1 topographic class, as per Eurocode-8 and NEHRP site class D, suggesting the risk for site amplification rather than the risk of topographic effects in such localities. The statistics of past earthquake events show that more than 47% of localities of large moment magnitude earthquakes ($M_w > 6.0$) have potentially experienced topographic effects (T2, T3, or T4 classes). Whereas, the SMN station sites are largely in the T1 class (~70% sites), unaffected by topographic amplification. The identified localities with topographic amplification can further be investigated for impact on probable seismic hazards and incident seismic waves using a numerical approach. The study also shows that for areas with complex physiography and heterogeneous landscape, the GIS-based procedure can be effectively utilized for preliminary identification of various landscape features and seismic site effects. The approach can be easily applied to any other region in the world. Moreover, the preliminary knowledge of expected topographic amplification can also help set up new recording stations for more comprehensive observation and recording of ground motion. The present study can be effective for efficient and strategic disaster management planning by identifying potential high amplification zones in terms of seismic hazard and selecting suitable sites for future infrastructural development.

Funding The authors declare that no funds, grants, or other support were received during the preparation of this manuscript.

Data availability The datasets generated during and/or analyzed during the current study are available from the corresponding author on reasonable request.

Declarations

Conflict of interest The authors have no relevant financial or non-financial interests to disclose.

References

Agrawal N, Gupta L, Dixit J (2021) Assessment of the socioeconomic vulnerability to seismic hazards in the national capital region of India using factor analysis. Sustainability 13(17):9652

Agrawal N, Gupta L, Dixit J (2022) Geospatial assessment of active tectonics using SRTM DEM-based morphometric approach for Meghalaya, India. All Earth 34(1):39–54

Allen TI, Wald DJ (2009) On the use of high-resolution topographic data as a proxy for seismic site conditions (VS30). Bull Seismol Soc Am 99(2A):935–943

Assimaki D, Gazetas G (2004) Soil and topographic amplification on canyon banks and the 1999 Athens earthquake. J Earthquake Eng 8(1):1–43

Association Française du Génie Parasismique (1990) AFPS 90, Recommendations for the redaction of rules relative to the structures and installations built in regions prone to earthquakes. French Association for Earthquake Engineering

Bouckovalas GD, Papadimitriou AG (2005) Numerical evaluation of slope topography effects on seismic ground motion. Soil Dyn Earthq Eng 25(7–10):547–558

Burrough PA, Mcdonnell RA, Lloyd CD (2015) Principles of geographical information systems. Oxford University Press, England

Cannon EC, Dutta U (2015) Evaluating topographically-derived Vs30 values for seismic site class characterization in. In: Proc. of the 6th international conference on earthquake geotechnical engineering, pp 2–4

Das S, Patel PP, Sengupta S (2016) Evaluation of different digital elevation models for analyzing drainage morphometric parameters in a mountainous terrain: a case study of the Supin-Upper Tons Basin. Indian Himalayas Springerplus 5(1):1–38

De Reu J, Bourgeois J, Bats M, Zwertvaegher A, Gelorini V, De Smedt P, Chu W, Antrop M, De Maeyer P, Finke P, Van Meirvenne M (2013) Application of the topographic position index to heterogeneous landscapes. Geomorphology 186:39–49

Del Gaudio V, Wasowski J (2011) Advances and problems in understanding the seismic response of potentially unstable slopes. Eng Geol 122(1–2):73–83

DeMets C, Gordon RG, Argus DF, Stein S (1994) Effect of recent revisions to the geomagnetic reversal time scale on estimates of current plate motions. Geophys Res Lett 21(20):2191–2194

Di Capua G, Lanzo G, Pessina V, Peppoloni S, Scasserra G (2011) The recording stations of the Italian strong motion network: geological information and site classification. Bull Earthq Eng 9(6):1779–1796

Dixit J, Dewaikar DM, Jangid RS (2012) Free field surface motion at different site types due to near-fault ground motions. ISRN Geophys 821051:1–6. https://doi.org/10.5402/2012/821051

Dixit J, Raghukanth STG, Dash SK (2016) Spatial distribution of seismic site coefficients for Guwahati city. In: Raju N (ed) Geostatistical and geospatial approaches for the characterization of natural resources in the environment. Springer, Cham. https://doi.org/10.1007/978-3-319-18663-4_80

Elyasi J, Bastami M, Kamalian M, Derakhshandi M (2021) Influence of the topographic effect on the seismic response of buried pipelines. Geoenviron Dis 8(1):1–14

EN 1998–5 (2004) Eurocode 8–design of structures for earthquake resistance, part 5: foundations, retaining structures and geotechnical aspects. European Committee for Standardization, Brussels. Online Available: https://www.phd.eng.br/wp-content/uploads/2014/11/en.1998.5.2004.pdf

Faccioli E, Vanini M, Frassine L (2002) Complex site effects in earthquake ground motion, including topography. In: 12th European conference on earthquake engineering (844). Barbican Centre, London, UK

Falcone G, Boldini D, Amorosi A (2018) Site response analysis of an urban area: A multi-dimensional and non-linear approach. Soil Dyn Earthq Eng 109:33–45

Falcone G, Boldini D, Martelli L, Amorosi A (2020a) Quantifying local seismic amplification from regional charts and site specific numerical analyses: a case study. Bull Earthq Eng 18(1):77–107

Falcone G, Mendicelli A, Mori F, Fabozzi S, Moscatelli M, Occhipinti G, Peronace E (2020b) A simplified analysis of the total seismic hazard in Italy. Eng Geol 267:105511

Gao Y, Zhang N, Li D, Liu H, Cai Y, Wu Y (2012) Effects of topographic amplification induced by a U-shaped canyon on seismic waves. Bull Seismol Soc Am 102(4):1748–1763

Gesch D, Oimoen M, Danielson J, Meyer D (2016) Validation of the ASTER global digital elevation model vol 3 over the conterminous United States. Int Arch Photogramm Remote Sens Spat Inform Sci 41:143

Grohmann CH, Riccomini C (2009) Comparison of roving-window and search-window techniques for characterising landscape morphometry. Comput Geosci 35(10):2164–2164

Gupta L, Dixit J (2022) A GIS-based flood risk mapping of Assam, India, using the MCDA-AHP approach at the regional and administrative level. Geocarto Int. https://doi.org/10.1080/10106049.2022.2060329

Gupta L, Agrawal N, Dixit J (2021) Spatial distribution of bedrock level peak ground acceleration in the national capital region of India using geographic information system. Geomat Nat Haz Risk 12(1):3287–3316

Gupta L, Agrawal N, Dixit J, Dutta S (2022) A GIS-based assessment of active tectonics from morphometric parameters and geomorphic indices of Assam region, India. J Asian Earth Sci X 8(1):100115

Hough SE, Altidor JR, Anglade D, Given D, Janvier MG, Maharrey JZ, Meremonte M, Mildor BSL, Prepetit C, Yong A (2010) Localized damage caused by topographic amplification during the 2010 M 7.0 Haiti earthquake. Nat Geosci 3(11):778–782

Hurukawa N, Tun PP, Shibazaki B (2012) Detailed geometry of the subducting Indian Plate beneath the Burma Plate and subcrustal seismicity in the Burma Plate derived from joint hypocenter relocation. Earth Planets Space 64(4):333–343

IS 1893 (2016), Criteria for Earthquake Resistant Design of Structures—General Provisions and Buildings Part-1, Bureau of Indian Standards, New Delhi

ISC (2021) International seismological centre, ISC-GEM earthquake catalogue 2021. http://doi.org/https://doi.org/10.31905/D808B825 [Accessed January 10, 2022]

Jafarzadeh F, Shahrabi MM, Jahromi HF (2015) On the role of topographic amplification in seismic slope instabilities. J Rock Mech Geotech Eng 7(2):163–170

Jenness J, Brost B, Beier P (2013) Land facet corridor designer. USDA forest service rocky mountain research station. http://www.jennessent.com/arcgis/land_facets.htm [Accessed January 10, 2022]

Karra K, Kontgis C, Statman-Weil Z, Mazzariello JC, Mathis M, Brumby SP (2021) Global land use/land cover with Sentinel 2 and deep learning. In: 2021 IEEE International geoscience and remote sensing symposium IGARSS pp 4704–4707

Kawase H, Aki K (1990) Topography effect at the critical SV-wave incidence: possible explanation of damage pattern by the Whittier narrows, California, earthquake of 1 October 1987. Bull Seismol Soc Am 80(1):1–22

Kayal JR, De R (1991) Microseismicity and tectonics in northeast India. Bull Seismol Soc Am 81(1):131–138

Khan S, Meijde MVD, Werff HVD, Shafique M (2020) The impact of topography on seismic amplification during the 2005 Kashmir earthquake. Nat Hazard 20(2):399–411

Kramer SL (1996) Geotechnical earthquake engineering. Pearson Education India, New Delhi

Kumar N, Narayan JP, Kumar V, Tiwari V (2021) Effects of shape and complexity of ridge topography on the comparative amplification scenario for the SH-and SV-waves. J Earth Syst Sci 130(1):1–20

Mascandola C, Luzi L, Felicetta C, Pacor F (2021) A GIS procedure for the topographic classification of Italy, according to the seismic code provisions. Soil Dyn Earthq Eng 148:106848–106848

Mittal H, Kumar A, Ramhmachhuani R (2012) Indian national strong motion instrumentation network and site characterization of its stations. Int J Geosci. https://doi.org/10.4236/ijg.2012.326117

Mokarram M, Roshan G, Negahban S (2015) Landform classification using topography position index (case study: salt dome of Korsia-Darab plain, Iran). Model Earth Syst Environ 1(4):1–7

Molina S, Lang DH, Singh Y, Meslem A (2019) A period-dependent topographic amplification model for earthquake loss estimation. Bull Earthq Eng 17(7):3709–3725

Monserud RA, Leemans R (1992) Comparing global vegetation maps with the Kappa statistic. Ecol Model 62(4):275–293

Nair HC, Joseph A, Gopinathan VP (2018) GIS Based landform classification using digital elevation model: a case study from two river basins of Southern Western Ghats. Modeling Earth Syst Environ 4(4):1355–1363

Nandy DR (2001) Geodynamics of Northeastern India and the adjoining region. Scientific book centre, Guwahati, Assam, Revised Edition 2017

Nath SK, Thingbaijam KKS, Adhikari MD, Nayak A, Devaraj N, Ghosh SK, Mahajan AK (2013) Topographic gradient based site characterization in India complemented by strong ground-motion spectral attributes. Soil Dyn Earthq Eng 55:233–246

NCS-MOES (2021) National center for seismology, ministry of earth sciences, government of India 2021. https://seismo.gov.in/MIS/riseq/ob_network; https://seismo.gov.in/MIS/riseq/earthquake/archive [Accessed January 10, 2022]

NTC2018 (2018) Norme tecniche per le costruzioni 2018, Il Ministro delle infrastrutture, Decreto 17 Gennaio 2018, 530

Pan H, Jiang X (2020) On the characteristics of ground motion and the improvement of the input mode of complex layered sites. Civil Eng J 6(5):848–859

Paolucci R (2002) Amplification of earthquake ground motion by steep topographic irregularities. Earthquake Eng Struct Dynam 31(10):1831–1853

Pessina V, Fiorini E (2014) A GIS procedure for fast topographic characterization of seismic recording stations. Soil Dyn Earthq Eng 63:248–258

Pham HT, Marshall L, Johnson F, Sharma A (2018) A method for combining SRTM DEM and ASTER GDEM2 to improve topography

estimation in regions without reference data. Remote Sens Environ 210:229–241
Pignalosa A, Forte G, Budetta P, Santo A (2022) Topographic amplification and debris remobilization as a cause for increasing rockfall hazard in seismic areas: a case study in Central Italy. Geomorphology 403:108160–108160
Poursartip B, Fathi A, Kallivokas LF (2017) Seismic wave amplification by topographic features: a parametric study. Soil Dyn Earthq Eng 92:503–527
Raghukanth STG, Dixit J, Dash SK (2011) Ground motion for scenario earthquakes at Guwahati city. Acta Geod Geoph Hung 46:326–346. https://doi.org/10.1556/AGeod.46.2011.3.5
Restrepo D, Bielak J, Serrano R, Gómez J, Jaramillo J (2016) Effects of realistic topography on the ground motion of the Colombian Andes-a case study at the Aburrá Valley. Antioquia Geophys J Int 204(3):1801–1816
Roy L, Das S (2021) GIS-based landform and LULC classifications in the Sub-Himalayan Kaljani Basin: Special reference to 2016 Flood. Egypt J Remote Sens Space Sci 24(3):755–767
Sandhu M, Sharma B, Mittal H, Chingtham P (2020) Analysis of the site effects in the North East region of India using the recorded strong ground motions from moderate earthquakes. J Earthquake Eng. https://doi.org/10.1080/13632469.2020.1724214
Sepúlveda SA, Murphy W, Jibson RW, Petley DN (2005) Seismically induced rock slope failures resulting from topographic amplification of strong ground motions: the case of Pacoima canyon. Calif Eng Geol 80(3–4):336–348
Shabani MJ, Ghanbari A (2020) Design curves for estimation of amplification factor in the slope topography considering nonlinear behavior of soil. Indian Geotech J 50(6):907–924
Tağıl Ş, Jenness J (2008) GIS-based automated landform classification and topographic, landcover and geologic attributes of landforms around the Yazoren Polje, Turkey. J Appl Sci 8:910–921
USGS (2021) US Geological survey national earthquake information center 2021 https://earthquake.usgs.gov/earthquakes/search/ [Accessed January 10, 2022]
Varade D, Sure A, Dikshit O (2019) Potential of landsat-8 and sentinel-2A composite for land use land cover analysis. Geocarto Int 34(14):1552–1567
Vinod PG (2017) Development of topographic position index based on Jenness algorithm for precision agriculture at Kerala. India Spatial Spatial Inf Res 25(3):381–388
Wald DJ, Allen TI (2007) Topographic slope as a proxy for seismic site conditions and amplification. Bull Seismol Soc Am 97(5):1379–1395
Weiss A (2001) Topographic position and landforms analysis. In:Poster presentation, ESRI user conference, San Diego, CA (Vol. 200)
Wilson JP, Gallant JC (2000) Terrain analysis: principles and applications. John Wiley and Sons, Hoboken